Spray Drop Size Characterization in an External-Mixing Bluff-Body Atomizer based on Acoustics and Multivariate Analysis

Raghav Sikka[a], Maths Halstensen[b], Joachim Lundberg[a]

[a]*Department of Process, Energy and Environmental Technology, University of South-Eastern Norway*

Raghav.Sikka@usn.no

[b]*Department of Electrical Engineering, IT and Cybernetics, University of South-Eastern Norway*

Maths.Halstensen@usn.no

Abstract

Air-assist atomizers have been widely used in various applications such as the aerospace industry, internal combustion engines, molten metal, food processing, etc. The mean drop size for these atomizers was obtained through the Shadowgraph imaging technique. This study aims to assess the feasibility of the acoustic chemometrics approach for classifying the atomizer types and predicting the mean drop size, such as Sauter mean diameter (SMD), for a two-phase spray atomizer employed. The droplet size measurements were carried out at three radial locations and one axial location for various air and liquid (water) flow rates. The acoustic signals were recorded through two different sensors: accelerometers and microphones. The main objective of this work is to implement prediction models for the mean drop sizes (SMD) measured at various locations. The model prediction is based on the dimensionless number B, whose unique values correspond to different two-phase flow working conditions. This analysis will further cater to the question that whether the acoustics chemometrics approach, including Principal Component Analysis (PCA) and Partial Least Squares Regression (PLS-R), is suitable for extracting valuable information such as predicting mean drop size (SMD) in two-phase flows through recorded acoustic signals.

Keywords: Acoustic Chemometrics, Multivariate Regression, Principal Component Analysis, Twin-fluid Spray, Mean droplet size

1. Introduction

Multi-phase flows can be found in various industrial applications ranging from fuel sprays in IC engines to petroleum pipelines. The most occurred case is two-phase flows in which gas and liquid interact to form various flow patterns generating vibrations and flow-based noise. Flow-based vibrations are classified into four types, in which acoustic resonance (flow-induced pulsations) and turbulent-induced excitation (FIV) are common in internal two-phase flows (Pettigrew and Taylor, 2016). Flow classification utilizing vibrations signals is present in literature (Miwa, Mori, and Hibiki, 2015). Flow rates and the vibration signals recorded using the PAT approach (sensors) showed a strong correlation (Evans, Blotter and Stephens, 2004). The peak frequency of these induced vibrations is proportionate to the flow parameters, such as void fraction (Ortiz-Vidal, Mureithi and Rodriguez, 2017). The time and frequency spectrum of the force fluctuations in two-phase flow were analyzed through flow-induced vibrations (Liu *et al.*, 2012). Though there are studies related to vibration-based analysis for flow classification, it lacks study on the effect of flow-induced vibrations (FIV) on the flow parameters such as local void fraction, interfacial area, and particle size distribution.

The single-phase flow (air only) can significantly affect the flow-induced vibrations and the acoustic noise. When expanded to high speeds, the jets produce shock-associated noise, further exacerbating flow-induced vibrations (Tam, 1998). The two-phase flow study constituting both vibration study for flow-induced vibrations caused due to internal flows and acoustic analysis from acoustic energy emitted from gas-liquid coaxial flows followed by two-phase mixing is still not considered. There have been attempts to measure the local two-phase flow parameters such as void fraction, Sauter mean diameter with flow-induced vibrations study (Hibiki and Ishii, 1998), and acoustic emission method (Guo et al. 2014). But the combination of techniques is still not attempted to date. This work applies a united approach, including accelerometers for acquiring flow-induced vibrations and microphones for obtaining acoustic signals. The novelty of this method lies in correlating the flow parameter, i.e., Sauter mean diameter (SMD), with acquired acoustic data and

parameter prediction using PLS-R. The data fusion with both techniques (described in the methods section) is done in the study to predict the flow parameter such as mean droplet size (SMD). The dual advantage of this approach is that vibrations, an inherent part of fluid flows in piping in industrial plants, can be used for both flow parameter prediction and dynamic stress analysis to estimate fatigue or structural damage.

2. Materials and Methods

The study was conducted utilizing the CMOS-based high-speed camera (Photron SA-Z), Nikon macro lens (80-200 mm), and Questar long-distance microscope (QM1). The rig setup built in-house at the process and energy department laboratory was used for the experiments. The different atomizers configuration with varying cone distances (L_c) and similar orifice (throat) diameters (d = 3.0 mm) were attached to the lance mounted at the Bosch Rexroth traverse system. Fig. 1 shows the airflow patterns for three atomizers.

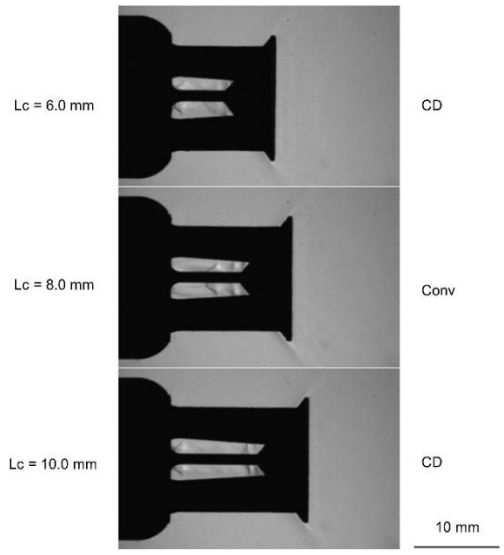

Figure 1: Airflow patterns in atomizers with three different cone distances (L_c)**.**

Yokogawa Rotamass and Endress Hauser Promass 83 (Coriolis type) flowmeter used water and air rate measurements. In the test rig (Figure 2), the compressor with 7.0 bar (g) capacity was employed for the air supply, and the water flow supply pump by Froster AS company was used. The water flow rate employed was 100, 200 and 300 kg/h, and the airflow rate employed are 20, 30 and 40 kg/h. Therefore, nine experiments were done at specific air-to-liquid mass ratios (ALR) and Weber number (We) based on liquid sheet velocity. The range of dimensionless number corresponds to ALR and the We number is mentioned in (Sikka, Halstensen and Lundberg, 2022)

ALR is defined as:

$$ALR = \frac{m_{air}}{m_{liquid}} \quad (1)$$

where mass flow rate in kg/hr.

Weber number is defined as:

$$We = \frac{\rho U^2 t}{\sigma} \quad (2)$$

A new dimensionless number (B) (depicted in Table 1) was employed, which is defined as:

$$B = We \cdot ALR \quad (3)$$

The experiments were conducted at STP such that fluid physical properties are assumed to be standard values. The spray formation in all three different cone distance (Lc) atomizers is illustrated in Fig. 2. The combined experimental setup for the spray imaging/drop size measurements and acoustic emission study is depicted in Fig. 3.

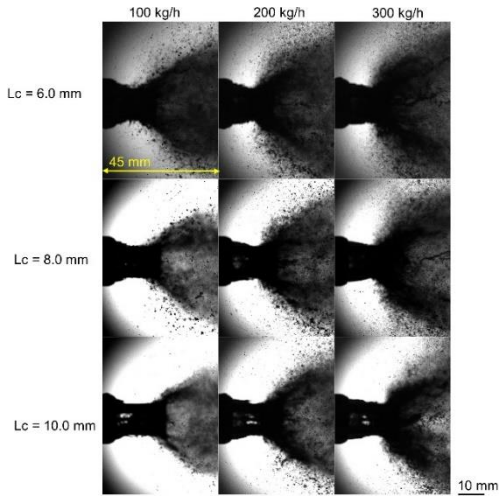

Figure 2: Images showing the spray pattern for 20 kg/h airflow rate at various liquid flow rates and the image size scaled (yellow line).

The acoustic arrangement employed two Piezoelectric types, 4518 accelerometers from Bruel & Kjær, Denmark, to collect noise/vibration data. Acoustic readings were procured using two electret condenser type Veco Vansonic PVM-6052-5P382 omnidirectional microphones (mounted on an arc at 300 mm from the spray centerline) with a sensitivity of -38 dB and signal-to-noise ratio of 58 dB. The microphone frequency ranges from 50 Hz to 16 KHz. The microphones were mounted along the arc at θ = 90º and 150º from perpendicular to the nozzle axis at R = 100D, termed "far-field" measurements (Wong et al., 2020). The vital point is that the acoustic data were recorded in a non- anechoic

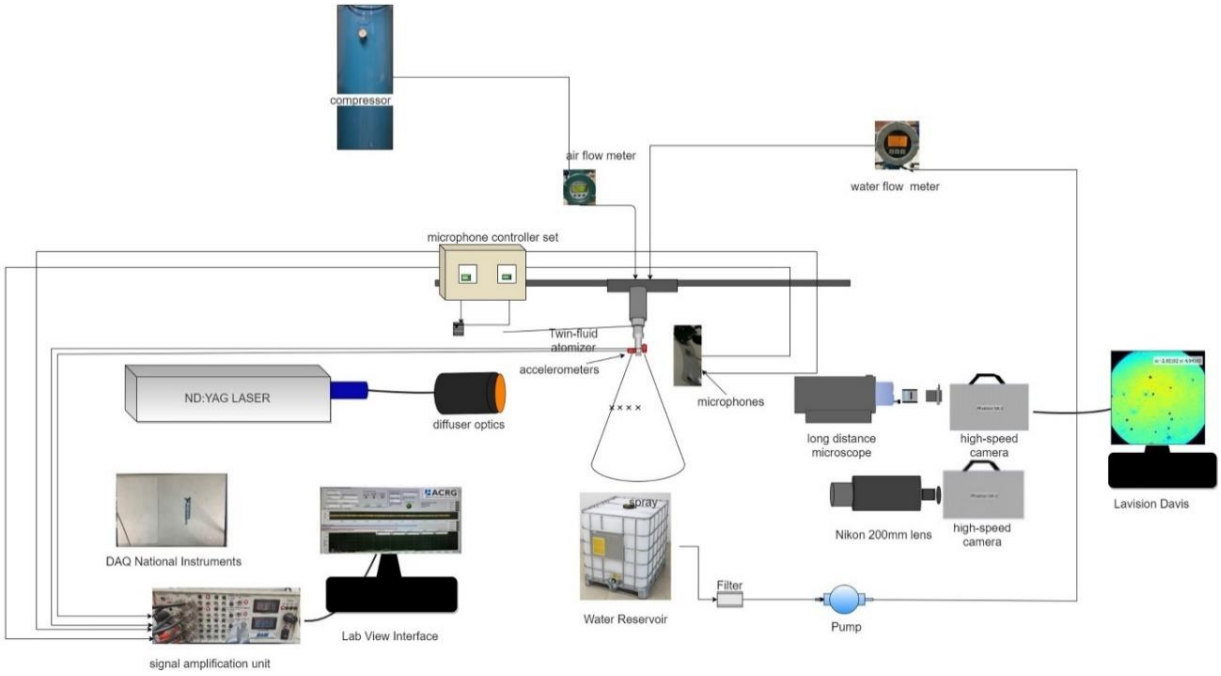

Figure 3: Schematic of the experimental setup for shadowgraphy technique along with the acoustic chemometric.

chamber, affecting the signal through stray noise. A data acquisition device (DAQ) from National Instruments (USB-6363), a signal amplification module, and a personal laptop with an in-house LabView interface was employed for signal acquisition. LabVIEW-based in-house created interface (Halstensen et al., 2019) was used for the acoustic chemometrics signal collection and signal conditioning. The signal processing was carried out on the acquired signal of 8192 recorded samples. The time-series signal was multiplied by a window (Blackman Harris) to avoid spectral leakage in the acoustic spectrum. This signal is finally transformed into the frequency domain using Discrete Fourier Transform. The Discrete Fourier Transform transforms a sequence of N complex numbers $\{x_n\}:= x_0,x_1,...,x_{n-1}$ into another sequence of complex numbers, $\{X_k\}:= X_0,X_1,...,X_{N-1}$, which is defined by equation (4):

$$X_k = \sum_{n=0}^{n-1} x_n \, e^{-i2\pi kn/N} \quad k = 0, \dots, N-1 \qquad (4)$$

A more advanced and efficient form of the DFT is the Fast Fourier Transform (FFT) (Ifeachor and Jervis, 1993), implemented for fast real-time calculations

2.1. Drop Size Measurements

The laser-based shadowgraphy method measured the mean drop size with a CMOS high-speed camera (Photron SA-Z model). The spray was illuminated by dual-cavity ND: YAG Laser (Photonics industries DM60-532 DH model) at 532 nm (green light). The uniform speckle-free light background was achieved with diffuser optics. Questar's long-distance microscope (QM1) provides a field of view (FOV) of 8.445 mm x 8.445 mm. The ParticleMaster software package incorporated in Davis 10.1 version (LaVision) is used for droplet sizing. The calibration plate provides a depth of field (DOF) of ~17:1. The minimum pixel used for particle

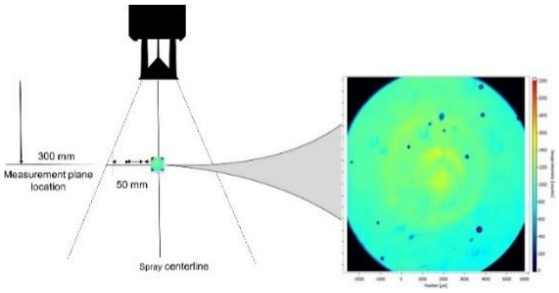

Figure 4: Schematic of the drop size measurement locations for shadowgraphy

detection is 3 pixels (in the area). The images were recorded at four locations depicted in Fig. 4 (line marked) – each 50 mm apart at the radial axis at 300 mm downstream from the outlet. Though, 500 images give convergence for mean droplet sizes. However, 1000 images were recorded for each measurement location which mitigates the measurement uncertainty (<1%). Laser intensity (in the current (A)) was set adequately to provide uniform background in proportion to the droplet

density of the shadowgraph picture. Note that the camera pixel resolution allowed for drop size measurements of 16−2000 µm. The mean drop size (SMD) for different radial locations is shown in Fig. 5.

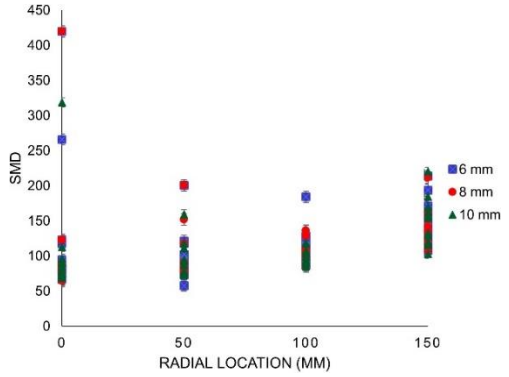

Figure 5: Mean drop size (SMD) for radial locations for all atomizers.

3. Results and Discussions

The acoustics spectrum is hard to analyze due to its multi-dimensional nature. Principal Component Analysis (PCA) is a dimensionality reduction technique that simplifies the analysis and reveals hidden patterns/structures. PCA projects the data into the new orthogonal plane, whose first principal component (PC1) is aligned in such a way that maximizes the variance. The new mean-centred plane is given by scores (T) and loadings (P) and residual (E). It is given by

$$X = T\,P^T + E \qquad (5)$$

The Nonlinear Iterative Partial Least Squares (NIPALS) algorithm developed (Wold, Esbensen and Geladi, 1987) was used for its many advantages. The method is unsupervised due to its independent Singular Value Decomposition (SVD) on the data.

The scores plot (Fig. 6) depicts how the acoustic spectrum was segregated as colour clusters for three different atomizers based on the tests carried out at various fluid flow rates. For the 6mm (L_c) atomizer, the maximum variance is in the first principal component (PC1) direction. Whereas for the 8 mm (L_c) atomizer, cluster points scattered in the PC2 direction show that PC2 contains valuable information. The loading plot (Fig. 7) shows that the information is there in all the frequencies for accelerometers, reflecting the PCA classification model capability. In contrast, for microphones, frequencies recorded are from a narrow spectrum.

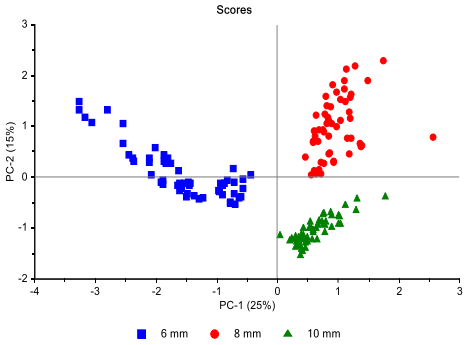

Figure 6: Score plot t1-t2 for all three atomizers.

The prediction model builds upon the regression-based method. Partial Least Squares regression (PLS-R) is a supervised method used to calibrate the predicting models, as explained in the PLS tutorial (Geladi and Kowalski, 1986).

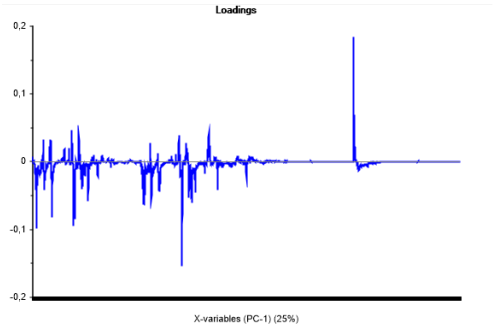

Figure 7: loadings plot for all the sensors.

PLS-R is a more advanced version of other regression techniques like MLR, PCR, etc. The robustness lies in the fact that model parameters vary little when new calibration samples are taken from the population. It builds on two-variable blocks, X and Y, representing training data. The NIPALS algorithm is used for PLS-R modelling (Halstensen, 2020). The X data matrix contains the frequency spectra in our study, and Y is a vector containing the mean drop size (SMD) values for a particular radial location. The regression model for mean drop size prediction is based on both accelerometers and microphone data.

The acoustic spectra used to calibrate the PLS-R model was a 162 x 8192 matrix, each sensor containing 162 frequency spectra. Each spectrum has 2048 frequencies ranging from 0 to 200 KHz for each sensor. The test set validation (50% data) was performed for alternate data values in the column. The root mean squared error of prediction (RMSEP) value, RMSEP (%) the slope, and the correlation coefficient (R^2) (Pearson) are commonly used in evaluating the different prediction models.

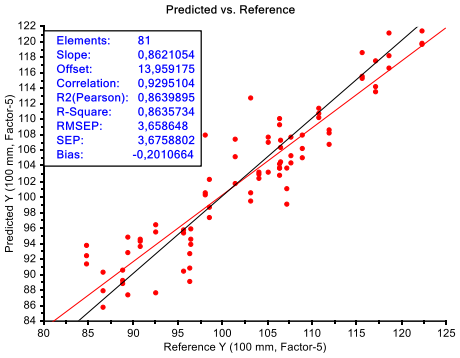

Figure 8: Predicted Vs. Reference (B) value. The target line (black) and regression line (red) are indicated.

The RMSEP is defined as

$$\text{RMSEP} = \frac{\sqrt{\sum_{i=1}^{n} \left(\hat{y}_{i,predicted} - y_{i,reference}\right)^2}}{n} \quad (3)$$

Where i = sample index number, n = total samples, RMSEP= Root Mean Squared Error of Prediction. The slope of 0.86 matches well with the target slope. RMSEP value comes out to be 3.65 with a correlation coefficient (R^2) value of 0.86 for a 100 mm location (Fig. 8). The loading weights linked the X matrix block to the Y-matrix through weights based on acoustic data (Fig. 9).

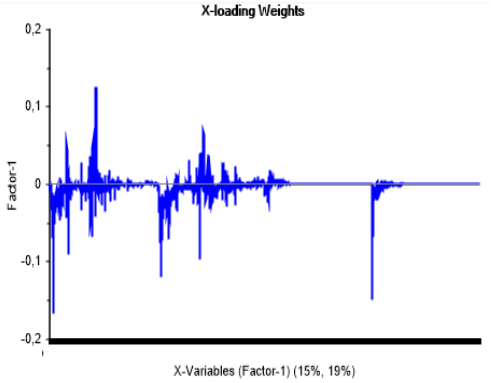

Figure 9: Loading weight plot for all sensors.

Table 1. Prediction models parameters

SMD Location	Prediction parameters (5 factors)			
	Slope	RMSEP	RMSEP (%)	R^2 Pearson
0 mm	0.74	7.22	12.2	0.75
50 mm	0.84	6.93	9.71	0.82
100 mm	0.86	3.65	9.60	0.86
150 mm	0.83	12.50	10.4	0.84

The prediction model parameters for all locations are given in Table 1.

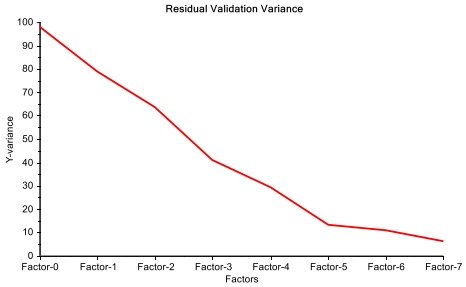

Figure 10: Residual validation variance plot.

Based on the residual validation variance plot (Fig. 10), the number of factors optimal for model prediction is 5, as Y-variance reduces drastically until 5 factors, then slightly decrease with more factors involved.

4. Summary

A feasibility study was conducted for the non-intrusive method using acoustic by applying multivariate data analysis techniques. The frequency data were recorded through accelerometers and microphones. The Principal Component Analysis (PCA) model reveals the clusters belonging to twin-fluid atomizers with the maximum variance in the first principal component (PC1) direction and first principal component (PC2) for the 6.0 mm cone distance (L_c) atomizer and 8.0 mm cone distance (L_c) atomizer, respectively. Prediction models based on the mean drop size (SMD) were fabricated using the Partial Least Squares regression (PLS-R) method. The prediction model works best for the 100 mm radial location as depicted by a low RMSEP (%) value of 9.60 and a high correlation coefficient (R^2) value of 0.86 when validated by test set validation.

References

Evans, R. P., Blotter, J. D. and Stephens, A. G. (2004) 'Flow rate measurements using flow-induced pipe vibration', *Journal of Fluids Engineering, Transactions of the ASME*, 126(2), pp. 280–285. doi: 10.1115/1.1667882.

Geladi, P. and Kowalski, B. R. (1986) 'PARTIAL LEAST-SQUARES REGRESSION: A TUTORIAL', *Analytica Chimica Acta*, (185), pp. 1–17.

Guo, M. *et al.* (2014) 'On-line measurement of the size distribution of particles in a gas-solid two-phase flow through acoustic sensing and advanced signal analysis', *Flow Measurement and Instrumentation*, 40, pp. 169–177. doi: 10.1016/j.flowmeasinst.2014.08.001.

Halstensen, M. (2020) 'Classification of Gases and Estimation of Gas Flow Rate Based on Unsupervised and Supervised Learning Respectively', (September), pp. 22–24. doi: 10.3384/ecp20176451.

Hibiki, T. and Ishii, M. (1998) 'Effect of flow-induced vibration on local flow parameters of two-phase flow', *Nuclear Engineering and Design*, 185(2–3), pp. 113–125. doi: 10.1016/s0029-5493(98)00241-6.

Hu, Y. *et al.* (2014) 'Online continuous measurement of the size distribution of pneumatically conveyed particles by acoustic emission methods', *Flow Measurement and Instrumentation*, 40, pp. 163–168. doi: 10.1016/j.flowmeasinst.2014.07.002.

Ifeachor, E. C. and Jervis, B. W. (1993) 'Digital signal Processing'.

Liu, Y. *et al.* (2012) 'Experimental study of internal two-phase flow induced fluctuating force on a 90° elbow', *Chemical Engineering Science*, 76(2012), pp. 173–187. doi: 10.1016/j.ces.2012.04.021.

Miwa, S., Mori, M. and Hibiki, T. (2015) 'Two-phase flow induced vibration in piping systems', *Progress in Nuclear Energy*, 78(2015), pp. 270–284. doi: 10.1016/j.pnucene.2014.10.003.

Ortiz-Vidal, L. E., Mureithi, N. W. and Rodriguez, O. M. H. (2017) 'Vibration response of a pipe subjected to two-phase flow: Analytical formulations and experiments', *Nuclear Engineering and Design*, 313, pp. 214–224. doi: 10.1016/j.nucengdes.2016.12.020.

Pettigrew, M. J. and Taylor, C. E. (2016) 'Two-Phase Flow-Induced Vibration : An Overview', 116(August 1994).

Sikka, R., Halstensen, M. and Lundberg, J. (2022) 'Characterization of the Flow (Breakup) Regimes in a Twin-Fluid Atomizer based on Nozzle Vibrations and Multivariate Analysis', in *62nd International Conference of Scandinavian Simulation Society, SIMS 2021, September 21-23, Virtual Conference, Finland*, pp. 22–27. doi: 10.3384/ecp2118522.

Tam, C. K. W. (1998) 'Jet noise: Since 1952', *Theoretical and Computational Fluid Dynamics*, 10(1–4), pp. 393–405. doi: 10.1007/s001620050072.

Wold, S., Esbensen, K. and Geladi, P. (1987) 'Principal Component Analysis', *Chemometrics and intelligent laboratory systems*, 2(1–3), pp. 37–52. Available at: http://files.isec.pt/DOCUMENTOS/SERVICOS/BIBLIO/Documentos de acesso remoto/Principal components analysis.pdf.

Wong, M. H. *et al.* (2020) 'Azimuthal decomposition of the radiated noise from supersonic shock-containing jets', *The Journal of the Acoustical Society of America*, 148(4), pp. 2015–2027. doi: 10.1121/10.0002166.